Theor Appl Climatol
DOI 10.1007/s00704-015-1589-5

ORIGINAL PAPER

WRF model evaluation for the urban heat island assessment under varying land use/land cover and reference site conditions

Shweta Bhati[1] · **Manju Mohan**[1]

Received: 30 January 2015 / Accepted: 23 July 2015

Abstract Urban heat island effect in Delhi has been assessed using Weather Research and Forecasting (WRF v3.5) coupled with urban canopy model (UCM) focusing on air temperature and surface skin temperature. The estimated heat island intensities for different land use/land cover (LULC) have been compared with those derived from in situ and satellite observations. The model performs reasonably well for urban heat island intensity (UHI) estimation and is able to reproduce trend of UHI for urban areas. There is a significant improvement in model performance with inclusion of UCM which results in reduction in root mean-squared errors (RMSE) for temperatures from 1.63 °C (2.89 °C) to 1.13 °C (2.75 °C) for urban (non-urban) areas. Modification of LULC also improves performance for non-urban areas. High UHI zones and top 3 hotspots are captured well by the model. The relevance of selecting a reference point at the periphery of the city away from populated and built-up areas for UHI estimation is examined in the context of rapidly growing cities where rural areas are transforming fast into built-up areas, and reference site may not be appropriate for future years. UHI estimated by WRF model (with and without UCM) with respect to reference rural site compares well with the UHI based on observed in situ data. An alternative methodology is explored using a green area with minimum temperature within the city as a reference site. This alternative methodology works well with observed UHIs and WRF-UCM-simulated UHIs but has poor performance for WRF-simulated UHIs. It is concluded that WRF model can be applied for UHI estimation with classical methodology based on rural reference site. In general, many times WRF model performs satisfactorily, though WRF-UCM always shows a better performance. Hence, inclusion of appropriate representation of urban canopies and land use–land cover is important for improving predictive capabilities of the mesoscale models.

1 Introduction

The phenomenon of urban heat island has now been established as an unwanted outcome of urban growth across the world. Urban heat island is classically defined as an urban area which is comparatively warmer than a surrounding rural area. This higher temperature is caused by human-induced modification of land surfaces leading to urban geometry which stores the short wave radiation (Oke 1982) as well as additional heat-generating activities associated with urban population (Oke 1973; Taha 1997). Along with urban centers of developed nations, the phenomenon is now prevalent in many Asian cities as well (Santamouris 2015). Urban heat island has been known to effect regional atmospheric pollution (Sarrat et al. 2006), ecology (Imhoff et al. 2010), extreme weather events and climate change (Tan et al. 2010; Emmanuel and Krüger 2012), energy consumption (Kolokotroni et al. 2012), and human comfort (Steeneveld et al. 2011).

Urban heat islands are studied through in situ experiments (Mohan et al. 2013; Mohan et al. 2012; Ren et al. 2007; Kolokotroni et al. 2006; Stewart 2011), remote observations (Weng et al. 2004, Yuan and Bauer 2007; Jin 2012), and numerical models. Numerical simulation of the urban heat island effect helps in increasing understanding of the phenomenon at region of interest, assessing major causative factors, and designing mitigation strategies. Over the years, numerical

✉ Manju Mohan
mmanju@cas.iitd.ac.in; mmohan6@hotmail.com

[1] Centre for Atmospheric Sciences, Indian Institute of Technology Delhi, Hauz Khas, New Delhi 110016, India

Published online: 08 August 2015

methods have evolved from simple energy budget model (Myrup 1969) to single and multi-layer urban canopy models (Kusaka and Kimura 2004; Kondo et al. 2005; Wang et al. 2013). These urban canopy models are integrated into global or mesoscale models. Examples include Community Land Model-Urban (CLM-U) in Community Atmospheric Model (Oleson et al. 2008; Ching 2013), Met Office Reading Urban Surface Exchange Scheme (MORUSES) in Met Office Unified Model (Porson et al. 2010), Town Energy Balance (TEB) in MesoNH model (Masson 2000), and the one which has been used in present study, the single-layer urban canopy model coupled with Weather Research and Forecasting (WRF) model (Chen et al. 2011a).

The WRF model is a commonly used mesoscale model which is now being used for various meteorological applications round the world including urban meteorology. Chen et al. (2014) simulated the urban heat island effect over Hangzhou City, China by WRF model coupled with an urban canopy model and found that peak of urban heat island effect was around 1,900 land surface temperatures (LST) around sunset with a magnitude of 1.6 °C. Giannaros et al. (2013) tested WRF model coupled with the Noah land surface model over the city of Athens, Greece for selected days during selected days and observed that the city of Athens gets about 4 °C warmer than its surroundings at night. Fallmann (2013) evaluated several urban parameterization schemes using WRF model to identify the urban heat island intensity for the urban region of Stuttgart, Germany and concluded that WRF is suitable for displaying regional climate patterns occurring through the difference between urban and rural environments. The study of urban heat island effect in India, however, is still in its initial stages. There have been studies based on observational data (Mohan et al. 2013; Mohan et al. 2012; Ramachandra and Kumar 2010; Khandelwal et al. 2010; Sundersingh 1990), but efforts still have to be undertaken to prepare a modeling framework for urban heat island effect for cities in Indian climate.

Further, there is the issue of selection of reference site for estimating heat island intensity. As per classical definition of urban heat island, it should be a rural location on the periphery of the city (Oke 1969). However, in India, many metropolitan cities are surrounded by growing satellite towns. Besides, with growth of urban population, many local rural sites in and around the city are rapidly being transformed into "urban villages" which are urban by nature because of compact built-up structures but still considered rural because of demographic lifestyle. Hence, it is often difficult to find a rural location, free of any urban influence, as a reference site for estimation of urban heat island intensity. This concern is being raised in some recent studies. Stewart and Oke (2009) and Stewart and Oke (2010) pointed that many urban heat island studies lacked a standardized description of "urban" and "rural" sites. They proposed 16 "local climate zones" based on sky view factor, spacing, vegetation fraction, building/tree height, etc. as a means to describe sites in a region as per a universal classification to facilitate reporting of results. Martin et al. (2014) argued that historical definition of urban heat island had relevance before the advent of satellite technology. Non-urban reference station could be located in a different biome and also vulnerable to frequent change in landscape due to farming activities thereby altering its surface energy exchange. Thus, instead of temperature difference between an urban and a reference rural site, intra-urban temperature variations within the city's administrative limits need more attention (Martin et al. 2014).

With this context, the present study attempts to utilize the WRF (v3.5) model coupled with single-layer urban canopy model to simulate the urban heat island scenario in the capital region of India. Urban heat island intensities (UHIs) have been computed based on model estimated temperatures which have been compared with in situ observations of numerous micro-meteorological stations in a field campaign carried out earlier (Mohan et al. 2013). Further study attempts to explore the selection of reference site for determining urban heat island intensity and applicability for in situ and WRF-simulated data.

2 Data and methodology

2.1 Study area

The study area of the National Capital Region of Delhi lies in the subtropical climate zone (Köppen classification: Cwa). Geologically, this region is bounded by the Indo-Gangetic alluvial plains in the north and east, by Thar Desert in the west, and by old Aravalli hill ranges in the south. There is a ridge trending along NNE–SSW direction which constitutes a small area of Delhi's terrain which is otherwise generally flat. Seasonally, the year can be divided into four main periods. Summer is experienced in the months of March–June followed by monsoon months of July, August, and September. Post-monsoon months are October and November, while the period of December–February constitutes the winter season. The maximum temperature ranges from 41 to 45 °C in peak summer season, and the minimum temperature in winter season is in the range of 3–6 °C in coldest period of December–January (Das 1968).

2.2 Model description

Weather Research Forecasting model (version 3.5) has been used in the present study. WRF is a compressible, Eulerian, and non-hydrostatic mesoscale model developed by NCAR (NCAR 2013; Skamarock et al. 2005). The model has diverse applications including weather prediction, data assimilation (Huang et al. 2009), regional climate modeling (Flaounas

et al. 2011; Leung and Qian 2009), and atmospheric chemistry (Gupta and Mohan 2013; Zhang et al. 2010; Tie et al. 2007). A single-layer urban canopy model (UCM) developed by Kusaka and Kimura (2004) has been coupled with WRF for better representation of surface energy balance in urban areas. The UCM consists of two-dimensional, symmetrical street canyons with simplified geometry of the buildings. The model estimates the surface temperature of roof, wall, and road surfaces as well as the fluxes from these surfaces (Tewari et al. 2007). The overview of a coupled Noah land surface model-WRF-UCM modeling system has been explained in detail in Chen et al. (2011a). Noah land surface model (LSM) provides surface-sensible and latent heat fluxes and surface skin temperature as lower boundary conditions for coupled atmospheric models. UCM coupling with Noah LSM in WRF is through the parameter urban percentage (or urban fraction, F_{urb}) that represents the proportion of impervious surfaces in the WRF sub-grid scale. For a given WRF grid cell, the Noah model calculates surface fluxes and temperature for vegetated urban areas (trees, parks, etc.), and the UCM provides the fluxes for anthropogenic surfaces. The total grid-scale sensible heat flux, for example, can be estimated as follows:

$$Q_H = F_{veg} \times Q_{Hveg} + F_{urb} \times Q_{Hurb}$$

where Q_H is the total sensible heat flux from the surface to the WRF model lowest atmospheric layer, F_{veg} is the fractional coverage of natural surfaces, such as grassland, shrubs, crops, and trees in cities, and F_{urb} is the fractional coverage of impervious surfaces, such as buildings, roads, and railways. Q_{Hveg} is the sensible heat flux from Noah for natural surfaces, and Q_{Hurb} is the sensible heat flux from the UCM for artificial surfaces. Grid-integrated latent heat flux, upward long wave radiation flux, albedo, and emissivity are estimated in the same way. Surface skin temperature is calculated as the averaged value of the artificial and natural surface temperature values and is subsequently weighted by their areal coverage (Chen et al. 2011a).

The simulation design consists of three domains (Fig. 1). The parent domain (D1) covers the Indian subcontinent with a spatial resolution of 18 km. The domain is a peninsular region flanked by Himalayan Mountains in the north. The first nested domain (D2) constitutes northern India region with resolution of 6 km. The second nested domain (D3), which is the area under analysis, covers the city of National Capital Region of Delhi and surroundings with a domain resolution of 2 km centered at 28.52° N and 77.12° E.

The simulation was carried out for time period of 5 March 2010 0000 UTC–11 March 2010 0000 UTC. First 24 h in simulation was considered as spin-up, and remaining hours were used for analysis. Physical parameterization schemes implemented in the model include Lin scheme (Lin et al. 1983) for microphysics, Rapid Radiative Transfer Model (RRTM) scheme for long wave radiation (Mlawer et al. 1997), Dudhia scheme for short wave radiation (Dudhia 1989), Noah land surface model (Tewari et al. 2004), Pleim-Xiu surface layer (Pleim 2006), Asymmetric Convection Model (ACM2) planetary boundary layer (Pleim 2007), and Kain-Fritsch cumulus parameterization (Kain 2004). With the exception of Noah land surface model, these schemes are based on best performing model options as recommended in Delhi region-based WRF sensitivity analysis by Mohan and Bhati (2011). Noah land surface model has been chosen because currently it is the only land surface scheme compatible with Moderate Resolution Imaging Spectroradiometer (MODIS) land use data. In the present study, MODIS land use data has been used for terrestrial mapping as it is more recent than the default United States Geological Survey (USGS) land use data. The MODIS Land Cover Type product is derived from observations spanning a year input of Terra and Aqua data. The land cover scheme used in WRF identifies 20 land cover classes defined by the International Geosphere Biosphere Program (IGBP). The dataset that comes with WRF is based on year 2001 (Ran et al. 2010). It has a resolution of 1 km and currently can be used only with Noah land surface model. NCEP final analysis data (FNL) of resolution 1° was used as input for initial and boundary conditions to the model.

Two sets of simulations were carried out. First, WRF was used without urban canopy model switched on. Then, urban canopy model was incorporated in WRF. For this purpose, some modifications were also required in the input land use/land cover data. Some urban stations of the field campaign had to be classified as low, medium, and high dense urban areas in the model domain. Building geometry parameters for urban canopy model (building height, building width, road width, etc.) were based on composite data from ground surveys, satellite images, and building bye-laws of the study region. Anthropogenic heat was turned off in the model for the present study. Simulations were thus carried out with modified land use and coupled with urban canopy model.

2.3 Observational data

A field campaign was conducted over the National Capital Region of Delhi to quantify and analyze the urban heat island effect in Delhi. The campaign has been described in detail in Mohan et al. (2013). Micrometeorological stations were set up at various sites throughout the Delhi region for continuous measurement of air temperature and relative humidity. There were 30 locations in the field campaign numbered from 1 to 30 where instruments were installed. These comprised of 27 sites where near surface temperature and relative humidity were measured. Three sites out of these (sites no. 2, 14, 17) also had a weather station (correspondingly numbered 3, 15, 18) installed at height of 10–15 m for measuring other

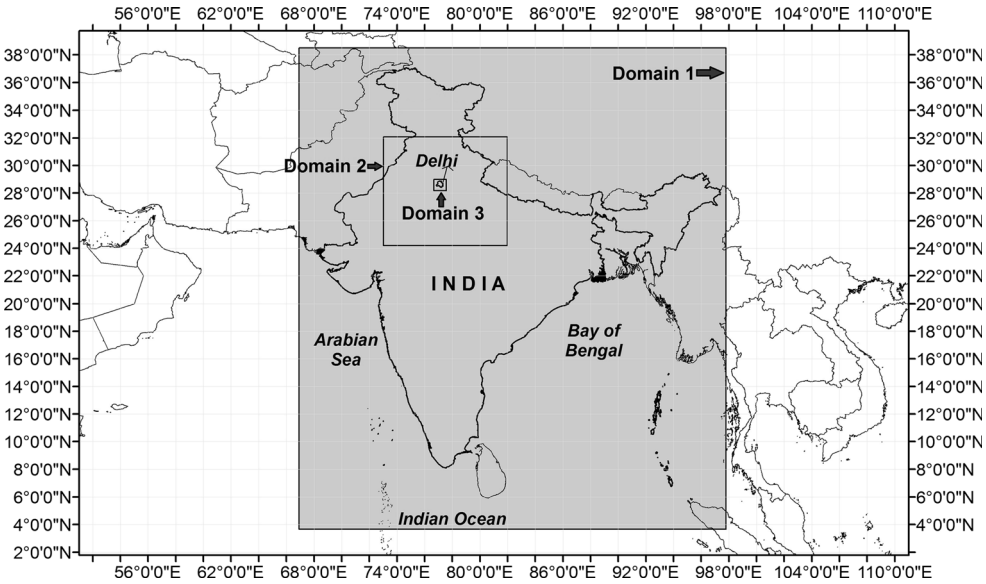

Fig. 1 Model domains

meteorological parameters like wind speed and direction, surface pressure, rainfall, and solar radiation along with air temperature. Data of weather stations have not been used for the present study. Further, instruments at station numbers 2 and 28 could not log quality data due to some technical and practical difficulties. Hence, sites whose data have been utilized for observational dataset of present study, include site nos. 1, 4–14, 16, 17, 19–27, 29, and 30. Out of these 25 sites, 19 are with urban characteristics while six are non-urban (Fig. 2). In addition, a rural site (Torni village, 28.24° N, 77.16° E) located about 40 km from periphery of Delhi city was chosen as reference site for computing urban heat island intensity. The rural site was a farmland free from any urban influence. Hereafter in the text, station names will be followed by their number in brackets. Measurements in this field campaign have been utilized as data for validation and evaluation of WRF model in the present study.

2.4 Evaluation methods

The present study deals with assessment of UHI. Hence, performance for WRF model has been analyzed for simulating near surface temperature and reproducing urban heat island intensity. Hourly averages for temperatures have been extracted from model outputs for location coordinates of stations in the field campaign. For the present study, the maximum distance between a model grid point and actual station location has come out to be 380 m. Simulated time series for near surface temperature have been compared with hourly averaged time series for observed temperatures. Further, UHIs have been computed (with respect to temperature at the reference rural site as mentioned in Section 2.3 above) from both observed temperatures as well as simulated temperatures followed by statistical evaluation. Statistical parameters such as mean bias (MB), mean absolute error (MAE), root mean-squared error (RMSE), correlation coefficient (CC), and index of agreement (IoA) have been determined for performance evaluation. While MB, MAE, and RMSE measure the error or deviation between observed and simulated values, correlation coefficient and index of agreement determine the degree to which magnitudes and signs of the observed value are related to the predicted values, in other words, the trend relationship (WMO 2008). As pointed out by Emery et al. (2001), evaluation of a meteorological model should be based on the performance that most models in past studies have been able to achieve. Based on their simulation experiments and literature review, they suggested gross error (also known as MAE) and index of agreement for evaluation of temperature estimations by meteorological models. The benchmark for temperature is that mean absolute error should be less than 2 °C and index of agreement should be greater than 0.8. These benchmarks have subsequently been used in many model performance evaluation studies (Borge et al. 2008; Gilliam and Pleim 2010, Shimadera et al. 2011; Hernández-Ceballos et al. 2013, Vázquez et al. 2014). In the present study also, the benchmarks proposed by Emery et al. (2001) have been used to for evaluation of model performance.

3 Results and discussion

Hereafter, simulations with only WRF model will be referred to as WRF, while simulations including urban canopy model also will be referred to as WRF-UCM.

3.1 Near surface air temperature

Time series of simulated near surface temperature (temperature at 2 m) versus observed temperatures are shown in Fig. 3.

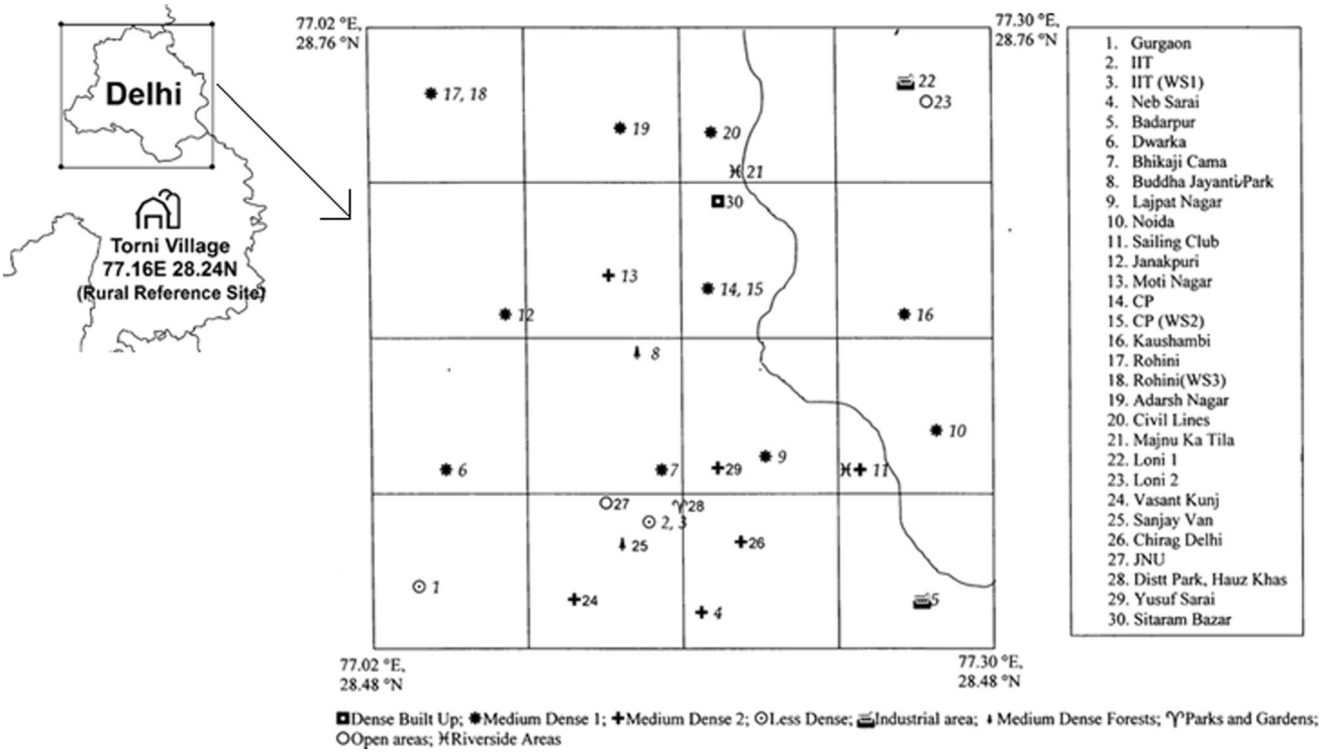

Fig. 2 Setup of micrometeorological stations in field campaign (Mohan et al. 2013)

Temperatures have been averaged separately for urban stations and non-urban stations (including rural reference site). In urban areas, both simulated time series show a trend of overestimation during daytime and underestimation during nighttime. However, for non-urban areas, WRF-simulated temperatures are mostly higher than observed temperatures. WRF-UCM temperatures are comparatively lower especially during daytime for both urban and non-urban areas. Thus, they are closer to the observed temperatures. Statistics for temperature are shown in Fig. 4. The bottom and top panels of Fig. 4 display mean absolute error and index of agreement, respectively. These statistics have been computed against temperature observed in field campaign. Maximum desirable mean absolute error and minimum desirable index of agreement as stipulated by Emery et al. (2001) are indicated by straight lines. With the exception of Loni-1, all stations have index of agreement above the least desirable value of 0.8 in WRF simulations. However, all stations show an index of agreement above 0.8 for WRF-UCM temperatures. Mean absolute errors for WRF-UCM temperatures are also lower than WRF for all temperatures and within desirable range barring just two stations. The model performance is comparatively weaker for certain non-urban areas like Buddha Jayanti Park, Sanjay Van, and Jawaharlal Nehru University (JNU)

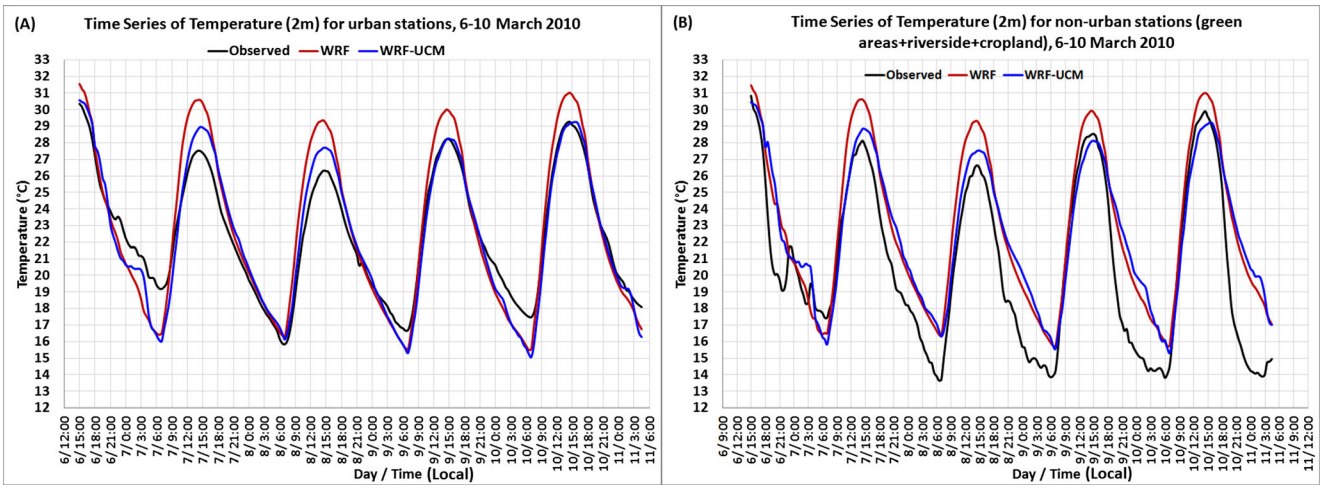

Fig. 3 Time series of near surface temperature (2 m). **a** Urban stations. **b** Non-urban stations

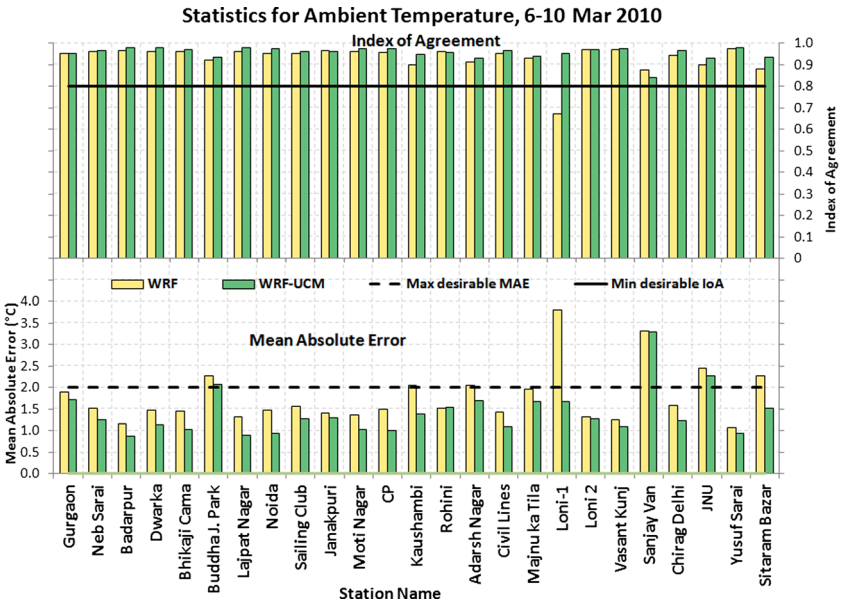

Fig. 4 Statistics for near surface temperature estimation by WRF model. *Top*: index of agreement. *Bottom*: gross error

even with WRF-UCM. Overall, with WRF-UCM, MAEs improve from 1.32 to 0.92 °C for urban areas and from 2.41 to 2.32 °C for non-urban areas. RMSEs improve from 1.63 °C (2.89 °C) to 1.13 °C (2.75 °C) for urban (non-urban) areas.

Figure 5 shows statistics for relative humidity for grouped urban and non-urban areas. Minimum desired index of agreement for relative humidity is 0.6 (Emery et al. 2001). While both WRF and WRF-UCM perform well for relative humidity, there is certainly an improvement in results with WRF-UCM. Table 1 lists the evaluation metrics of some earlier studies using urban canopy model. The values of the present study also lie within the range of those obtained in past studies. Thus, based on statistical indicators, overall model performance at various urban sites is inferred to be reasonably good.

3.2 UHI

3.2.1 UHI for different LULC

Figure 6 displays diurnal time series of UHI for four different land use/land cover (LULC) averaged over the duration of field experiment. UHIs have been calculated with reference to an external rural site as mentioned in Section 2.3. Generally, without inclusion of urban canopy model, simulated UHI for urban built-up areas was found to be higher than observed UHI in daytime and vice versa during nighttime. As can be seen in Fig. 3, the model overestimates temperature during daytime but underestimates in nighttime for urban stations. However, temperatures are overestimated throughout the day for the non-urban areas. Thus, in nighttime, the difference between temperature at a site and reference rural site will be higher for observed temperatures than simulated temperatures. During daytime, temperatures for both urban and non-urban are being overestimated to various degrees and thereby leading to higher UHI for all sites. As in the case of temperature, model performance for reproducing UHI is poorest for green areas.

However, with urban canopy model, simulated UHIs come closer to observed UHIs during both daytime and nighttime. Similarly, modification of land use to correctly represent non-urban areas has led to improvement in green and riverside areas especially during daytime.

Table 2 presents statistical evaluation of UHI computed based on WRF and WRF-UCM using parameters such as MB, MAE, RMSE, CC, IoA, and hit rate. Hit rate has been

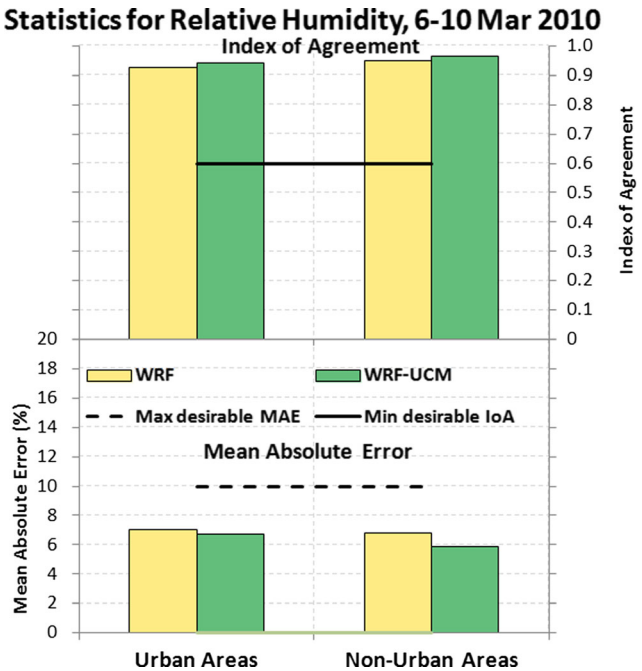

Fig. 5 Statistics for near surface relative humidity. *Top*: index of agreement, *Bottom*: gross error

Table 1 Statistics of some earlier studies using urban canopy model

Study	Region	Met variable	Parameter	Value
Chen et al. (2014)	Hangzhou City, China	2-m mean temperature	RMSE	1.22
Giannaros et al. (2013)	Athens, Greece	Near surface temperature	IoA	0.88 to 0.95
			RMSE	1.29 to 1.85
Kim et al. (2013)	Greater Paris	Temperature	Bias	−2.91 to 0.94
			RMSE	2.39 to 3.99
Lee et al. (2012)	Chuncheon, Korea	Temperature	RMSE	1.38 to 1.67
Kusaka et al. (2012a, 2012b)	Tokyo metropolitan area	Surface air temperature	Bias	−1.2 °C
			RMSE	2.7 °C
		Relative humidity	Bias	2.2 %
			RMSE	7.8 %
Chen et al. (2011b)	Greater Houston Area	Near surface temperature	IoA	0.97
			RMSE	1.44
		Relative humidity	IoA	0.84
			RMSE	17.64
Wang et al. (2009)	Pearl River Delta and Yangtze River Delta Regions	2-m temperature	MAE	1.8
			RMSE	2.3
		2-m RH	MAE	10.5
			RMSE	13.5
Zhang et al. (2008)	Chongqing, China	Surface air temperature	Bias	2.43
			RMSE	0.55
		Relative humidity	Bias	−22 %
			RMSE	2.55 %
Present study	National Capital Region of India (Delhi and surroundings)	Surface air temperature	IoA	0.89 to 0.97
			RMSE	1.1 to 3.2
		Relative humidity	IoA	0.78 to 0.96
			RMSE	7.0 to 16.3

computed as percentage of simulated UHIs with a value within ±2 °C of corresponding observed UHI (Cox et al. 1998). Thus, hit rate serves as an indicator of models' ability to capture in situ UHI magnitudes. Performance of WRF and WRF-UCM for temperature is closely associated with their performance for UHI as well. As shown in Fig. 4, statistical indices for evaluation of WRF temperatures are within acceptable ranges for all urban areas but not so for non-urban areas. In the same way, WRF is able to capture mean UHIs for urban areas much better (hit rate=72 %) in comparison to riverside areas, open areas, or green areas (hit rate=52 %). However, overall model performance for UHI improves significantly with WRF-UCM. WRF-UCM is able to capture mean UHIs best for urban areas (hit rate=75 %) followed by river side areas (73 %), green areas (hit rate=71 %), and open areas (hit rate=67 %).

Simulated UHIs in the present study seem reasonable when compared to past studies. Giannaros et al. (2013) estimated maximum urban heat island intensity of 4.6 °C against observed UHI of 5.7 °C in Athens City, Greece using WRF model and land surface temperature assimilation. Hu et al. (2013) estimated maximum UHI ranging from about 2.0 to 2.5 °C for an observed value of about 2.2 °C in Oklahoma City, and Meng et al. (2011) determined a value of about 3 °C for maximum observed UHI of about 3 °C.

Table 3 represents summary of maximum urban heat island intensity for each day of the experimental field campaign. The table displays magnitude of maximum observed and simulated (WRF-UCM) urban heat island intensity and time period of its occurrence during both night hours as well as day hours. During the entire field campaign, maximum daytime observed UHI is 8.2 °C, while maximum simulated UHI is 7.5 °C. In nighttime, the observed peak UHI is 10.7 °C, while simulated value is 7.3 °C. During daytime, the peaks occur at the same time in both measurements and model estimations. The absolute difference in magnitudes of peaks lies between 0.2 and 2.5 °C. In nighttime, the difference between occurrences of peaks is usually 2–4 h. The absolute difference in magnitudes of peaks ranges from 0.1 °C (7–8 March) to 3.6 °C (10–11 Mar). Numbers of stations which are common among top

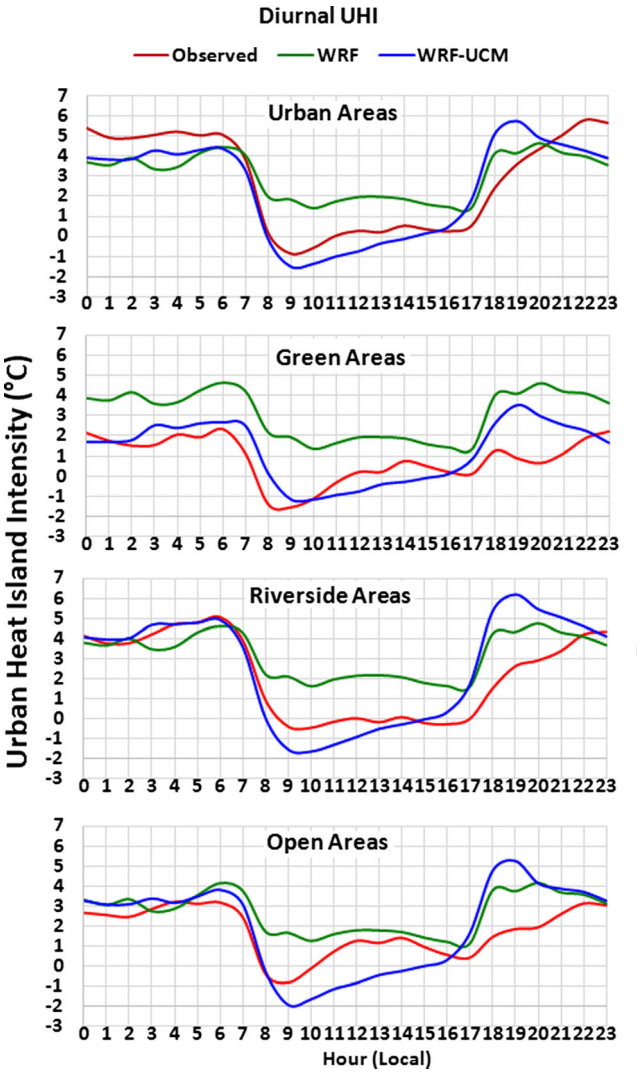

Fig. 6 Diurnal range of UHI for different land use land cover types

three stations in terms of UHI magnitude at peak times are also stated in Table 3. Location of top three stations in terms of UHI magnitude is largely similar for nighttime but not in the case of daytime.

3.2.2 Selection of reference point

As discussed in Section 1, cities are fast expanding into urban agglomerations with main city at the center and satellite towns surrounding it. Hence, it is becoming increasingly difficult to find a rural area free of urban influence to serve as a reference site. Cities like Delhi have a highly mixed land use with many non-built-up zones within the city (parks, shrublands, etc.) which are usually cooler than built-up areas. Thus, there is also an option to keep a green site within the city as a reference point.

In field experiments conducted in year 2010, this issue was addressed by estimation of UHI by two approaches (Mohan et al. 2013). The first approach was to estimate UHI using the classical approach as temperature difference between a site and a rural location ($\Delta T_{\text{site-rural}}$). For this purpose, a village site (Torni village) located at a distance of about 40 km from study region was chosen as reference site. The second approach was to estimate UHI as a difference between temperature at a site and the lowest temperature among all sites within a study region at a given hour ($\Delta T_{\text{site-min}}$). It was found out that UHI estimated from both methods was fairly in agreement with each other. In the present study, these two approaches have been applied for UHI estimations from WRF-simulated temperatures. Figure 7(a) displays time series of maximum hourly UHI computed from these two approaches for both observed and WRF temperatures. It can be seen that unlike for observed temperatures, there is a significant difference

Table 2 Statistical analysis of simulated UHI

Land use/land cover	UHI	Mean bias		MAE		RMSE		CC		IoA		Hit rate	
		W	U	W	U	W	U	W	U	W	U	W (%)	U (%)
Urban	Mean	−0.36	−0.17	1.50	1.24	1.91	1.60	0.65	0.80	0.77	0.88	72	75
	Max	−1.00	−0.96	1.79	1.51	2.39	1.87	0.65	0.84	0.73	0.88	65	65
	Min	1.28	0.66	1.72	1.43	2.02	1.78	0.59	0.63	0.66	0.75	55	71
Green areas	Mean	2.02	0.44	2.09	1.17	2.52	1.55	0.55	0.49	0.52	0.68	52	71
	Max	1.05	1.03	1.48	1.73	1.98	2.24	0.54	0.62	0.67	0.72	63	65
	Min	2.98	−0.14	3.04	1.15	3.44	1.59	0.40	0.34	0.43	0.60	26	76
Riverside	Mean	0.72	0.56	1.52	1.28	1.85	1.74	0.64	0.78	0.76	0.86	65	73
	Max	0.51	0.29	1.53	1.33	1.86	1.71	0.62	0.78	0.75	0.87	61	74
	Min	0.94	0.84	1.58	1.38	1.95	1.89	0.63	0.76	0.74	0.83	56	71
Open areas + croplands	Mean	0.73	0.45	1.25	1.47	1.63	1.84	0.55	0.59	0.68	0.70	74	67
	Max	0.41	0.39	1.23	1.51	1.59	1.84	0.60	0.70	0.76	0.79	74	66
	Min	1.04	0.50	1.45	1.62	1.91	2.04	0.44	0.38	0.58	0.57	65	64

W WRF, *U* WRF-UCM

Table 3 Comparison of time and magnitude of maximum UHI

		Day →	6 March	7 March	8 March	9 March	10 March
Daytime UHI	Peak time	Obs	NA	7:00	7:00	7:00	17:00
		WRF	–	7:00	7:00	7.00	17:00
	Magnitude (°C)	Obs	NA	5.0	7.5	8.2	2.4
		WRF	–	4.54	7.3	5.7	2.7
	Common top 3 UHI stations		–	2	1	1	2
		Night →	6–7 March	7–8 March	8–9 March	9–10 March	10–11 March
Nighttime UHI	Peak time	Obs	21:00	5:00	4:00	23:00	23:00
		WRF	19:00	5:00	1:00	19:00	19:00
	Magnitude (°C)	Obs	7.8	7.4	8.1	8.8	10.7
		WRF	6.1	7.3	6.6	6.9	7.1
	Common top 3 UHI stations		3	3	2	3	2

between time series of UHI computed by two methods for model-simulated temperatures. In the observed dataset, minimum temperatures were usually recorded in green areas. Hence, in the second approach, UHI was calculated usually with respect to temperature of a green area. However, this has not been captured in simulated temperatures. Table 1 also showed that the model does not perform well for green areas. Consequently, there is a huge difference between time series of $\Delta T_{\text{site-min}}$ for observed and simulated temperatures. In contrast, time series for $\Delta T_{\text{site-rural}}$ for observed and simulations are in close agreement with each other. The difference between observed and simulated UHIs of all the stations and days combined with respect to minimum temperature at green area site ranges from 0.5 to 8.3 °C with an average of 5.2 °C. The corresponding difference in UHIs with respect to rural site as reference ranges from −2.3 to 6.7 °C but with an average absolute difference of 1.7 °C.

On the other hand, UHIs based on WRF-UCM simulations from both methods are much closer to observed UHIs (Fig. 7(b)). Even UHIs computed by $\Delta T_{\text{site-min}}$ have improved significantly.

Table 4 lists correlation coefficients between series of observed and simulated UHIs computed by both methods. UHIs from WRF-UCM simulations are in close agreement with observed UHIs for both minimum temperature site reference approach (CC=0.80) and rural site reference approach (CC= 0.82). The prime reason of discrepancy between $\Delta T_{\text{site-min}}$ and $\Delta T_{\text{site-rural}}$ is incorrect representation of LULC of non-urban areas in the model which gets corrected to some extent when urban canopy model is turned on with WRF with modification of LULC.

Figure 8 represents LULC over the study area as simulated in the model at a resolution of 2 km. As stated earlier, MODIS land use data has been used in the model for terrestrial mapping which has a resolution of 1 km. However, the process of mapping over model domain of 2 km (innermost domain) considers only the most dominant LULC in a particular 2× 2-km grid cell. Thus, if a non-urban site is in a vicinity of large urban area, it comes under urban category during the terrestrial mapping of the model. As can be seen in Fig. 8a, almost all the stations lie in urban built-up class. This greatly impacts the model performance for non-urban areas. Hence, intra-city heat islands are markedly different from urban–rural heat islands in simulated temperatures. However, with the inclusion of UCM along with appropriate land use changes for certain stations (Fig. 8b), LULC of the model domain comes closer to actual LULC. This improves model performance for all stations which causes UHIs from both methods to be in agreement with each other. Hence, if the LULC of the stations is correctly being represented in the model, reference point for UHI estimation can be chosen within the city. A minimum temperature site (such as a green area) within the city can serve as a reference point instead of a rural site outside the city. This approach can be considered for methodological aspects for conducting future UHI studies in cities like Delhi which have highly mixed land use–land cover. However, this needs to be explored in other cities for general applicability.

3.2.3 Spatial distribution of UHI

Figures 9, 10, and 11 display spatial distribution of "relative urban heat island intensity" over the study area. Relative heat island intensity is a measure of standardized urban heat island intensity. A dissimilar range of values (minimum to maximum range) often experienced in any two given data sets may not bring out the common features of contours and hotspots in spatial distribution plots when compared. Analogously, the range of UHI estimated based on observations may be quite different than the UHI obtained from the model simulations, and spatial contours may not bring out the common features of distributions and hotspots. Thus, to overcome comparison with dissimilar range of values in spatial distribution plots of observed and simulated UHI values, a non-dimensional scaling parameter termed as relative heat island intensity is

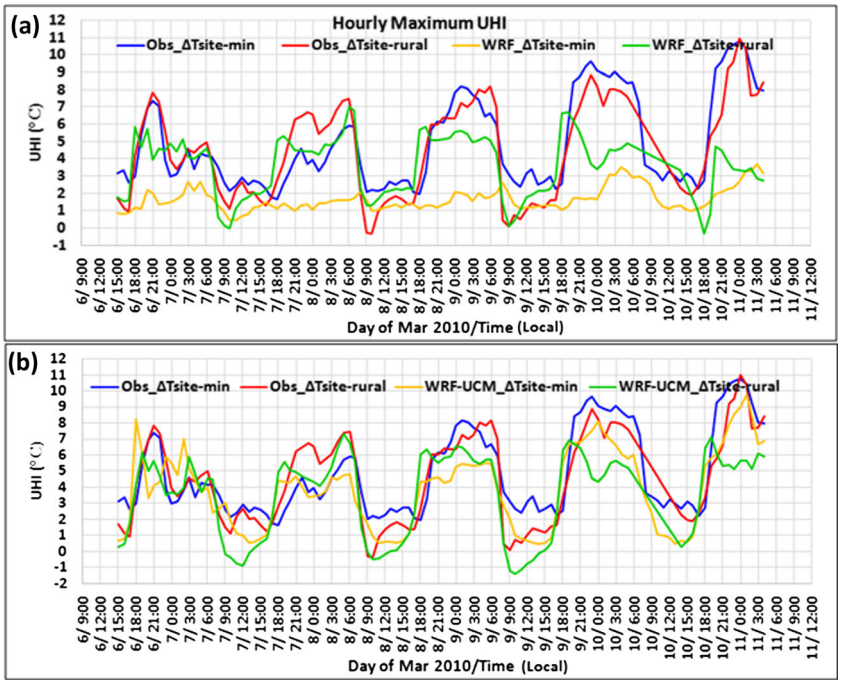

Fig. 7 Hourly maximum UHI computed by two methods. **a** Comparison with WRF. **b** Comparison with WRF-UCM

proposed in this study. Relative UHI helps in determining whether the model was able to capture high UHI zones or not or how good is the distribution pattern of simulated UHI when compared with the observed hotspots. Relative UHI is defined as

$$\text{Relative UHI}(x,y) = \frac{\text{UHI}(x,y)}{D}$$
$$D = \max|\text{UHI}(x_i,y_i)|$$

where relative UHI of a point x,y in a domain is estimated by dividing UHI at that point with a standardizing factor D. D is the maximum of absolute values of UHIs of all points (x_i,y_i) in the given domain. By using relative UHI, a uniform scale of −1 to +1 can be applied to the spatial distribution. A negative value of relative UHI implies cool islands.

UHI based on air temperatures Nighttime (0300 hours) (Fig. 9): Three major hotspots were observed in the field campaign for nighttime. These were the commercial or highly dense urban sites of Sitaram Bazar (30), Connaught Place (CP) (14), and Bhikaji Cama (7). Maximum observed UHI is 6.4 °C in Sitaram Bazar (30)–CP (14) zone. The corresponding WRF-simulated UHI at same location is lower with a magnitude of 4.5 °C. However, from relative UHI distribution (Fig. 9), we can see that top UHI hotspots in observed spatial contours are also captured in simulated UHI distribution.

The inclusion of urban geometry in the model with UCM increases the maximum UHI to 5.4 °C. Some cool zones are also observed in WRF-UCM distribution with modification of land use. Urban geometry plays a crucial role during nighttime by being a significant contributor in outward surface fluxes. This results in increasing the magnitude of consequent UHI also in WRF-UCM distribution.

Table 4 Correlation coefficient matrix of observed and simulated UHIs computed by two methods

UHI→ ↓		Observed		WRF		WRF-UCM	
	Approach→ ↓	$\Delta T_{\text{site-min}}$	$\Delta T_{\text{site-rural}}$	$\Delta T_{\text{site-min}}$	$\Delta T_{\text{site-rural}}$	$\Delta T_{\text{site-min}}$	$\Delta T_{\text{site-rural}}$
Observed	$\Delta T_{\text{site-min}}$	1					
	$\Delta T_{\text{site-rural}}$	0.88	1				
WRF	$\Delta T_{\text{site-min}}$	0.67	0.60	1			
	$\Delta T_{\text{site-rural}}$	0.37	0.64	0.30	1		
WRF-UCM	$\Delta T_{\text{site-min}}$	0.80	0.84	0.58	0.47	1	
	$\Delta T_{\text{site-rural}}$	0.67	0.82	0.42	0.60	0.83	1

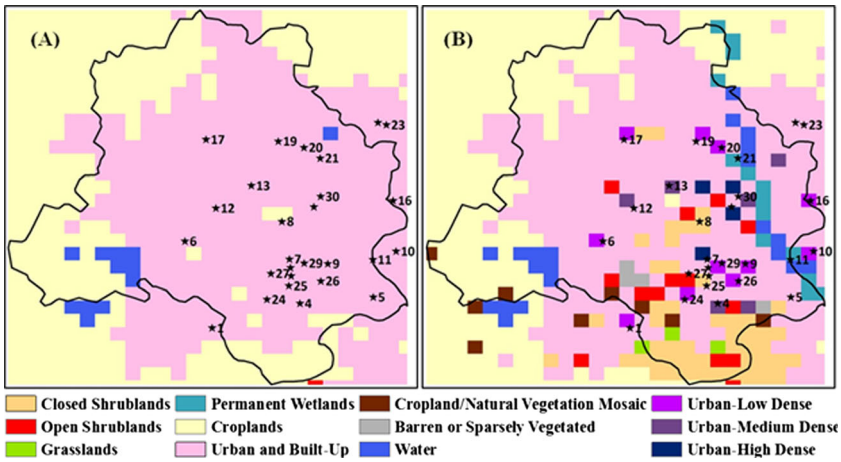

Fig. 8 Land use of Delhi as simulated by WRF based on MODIS land use data with (**a**) WRF (**b**) modified LULC with UCM. * symbols followed by number indicate location of micrometeorological stations and their station code in the field campaign with actual LULC depicted in Fig. 2

Daytime (1500 hours): Unlike nighttime, magnitudes of WRF-estimated UHIs are higher than observed UHIs. The maximum observed UHI is 2.2 °C, while maximum simulated UHI is 2.4 °C. However, there are no distinct hotspots in simulated UHI distribution (Fig. 10). There are a number of stations which fall under same UHI range. Among both figures, only Badarpur (5) station is the one with similar UHI range and location. However, daytime UHI spatial distribution for WRF-UCM is in much closer agreement with observed UHI distribution. Both cool spots Buddha Jayanti Park (8) as well as hot spots (Janakpuri (12) and Badarpur (5)) have emerged clearly in WRF-UCM distribution. The maximum UHI (2.3 °C) is also slightly lower than that of WRF. Overall nighttime UHI magnitudes are higher than daytime.

Surface heat island Figure 11 displays spatial distribution of relative surface heat island intensity (SHI). The observed SHI in this case has been computed based on LST retrieved from

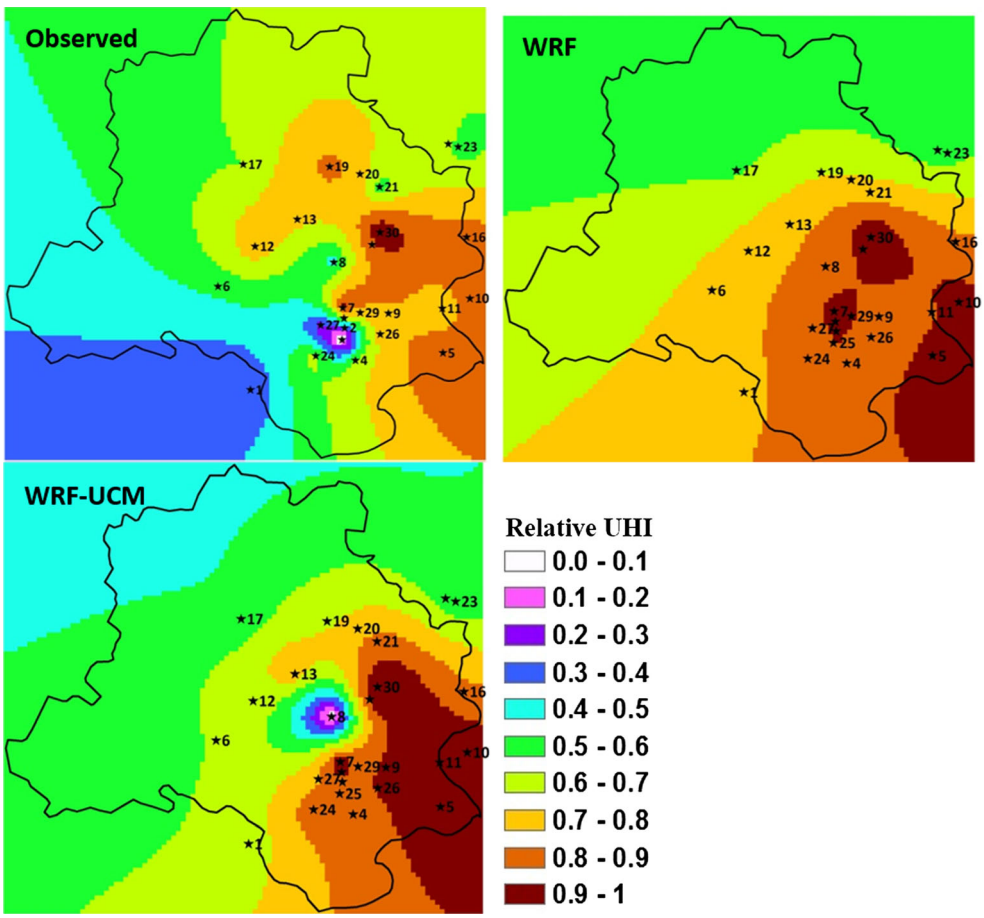

Fig. 9 Spatial distribution of nighttime relative UHI [Max UHI Obs: 6.47 °C; WRF: 4.59 °C, WRF-UCM: 5.36 °C]

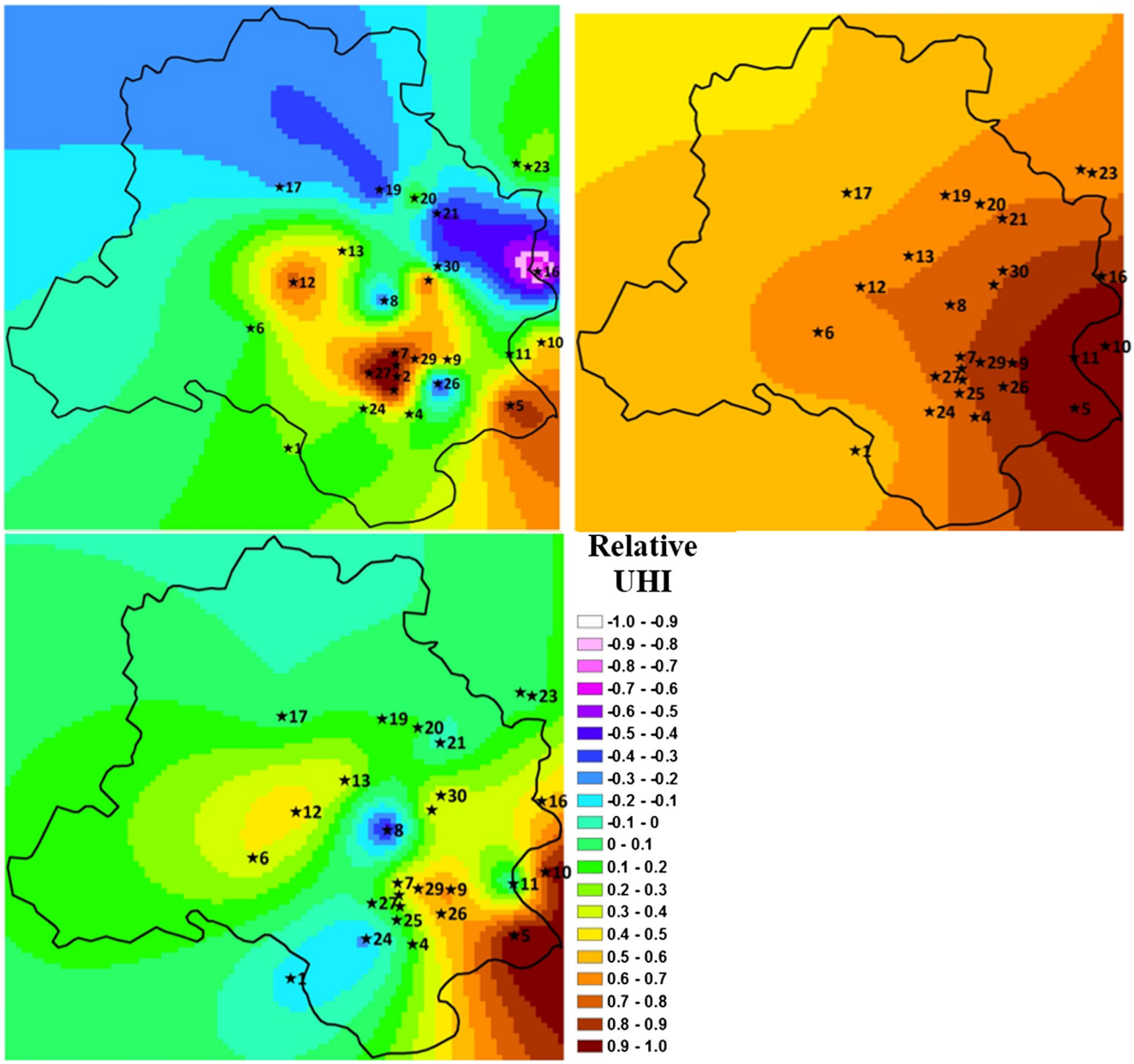

Fig. 10 Spatial distribution of daytime relative UHI [Max UHI Obs: 2.2 °C; WRF: 2.4 °C, WRF-UCM: 2.3 °C]

MODIS Terra satellite. MODIS LST data are available as 8-day averaged land surface temperatures with resolution of 1 km (Giovanni 2014). The 8-day segment of the satellite land product (March 6–March 13) coincides with field experiment dates (March 6–March 11), and thus simulated temperatures have been averaged for the experiment duration.

Hotspots are distinct and prominent in both daytime as well as nighttime observed spatial plots but not in simulated relative SHI spatial plots. Simulated UHI zones are more spread rather than concentrated. Chen et al. (2014) observed something similar in one of the sensitivity runs that were performed for examining impact of urbanization-caused surface changes and anthropogenic heat on heat islands. It was observed that the UHI intensity for the land surface temperature was significantly larger than that for the 2-m air temperature and the UHI extended over an area of approximately the same horizontal size of the urban land use. Maximum SHI for nighttime is 7.6, 7.5, and 6.2 °C for observed, WRF, and WRF-UCM distributions, respectively. No hotspots are captured for daytime, and the domain is generally cool with negative relative SHI. This implies that the rural reference site has higher LST. This phenomenon is commonly referred to as the negative heat island in which the city surface acts as an urban heat sink (Giannaros et al. 2013; Keramitsoglou et al. 2011). Observed SHIs are generally higher than simulated SHIs. The model estimates surface skin temperature, while MODIS measures the thermal radiation emitted from the surface. Ding and Shi (2013) observed that rooftops in

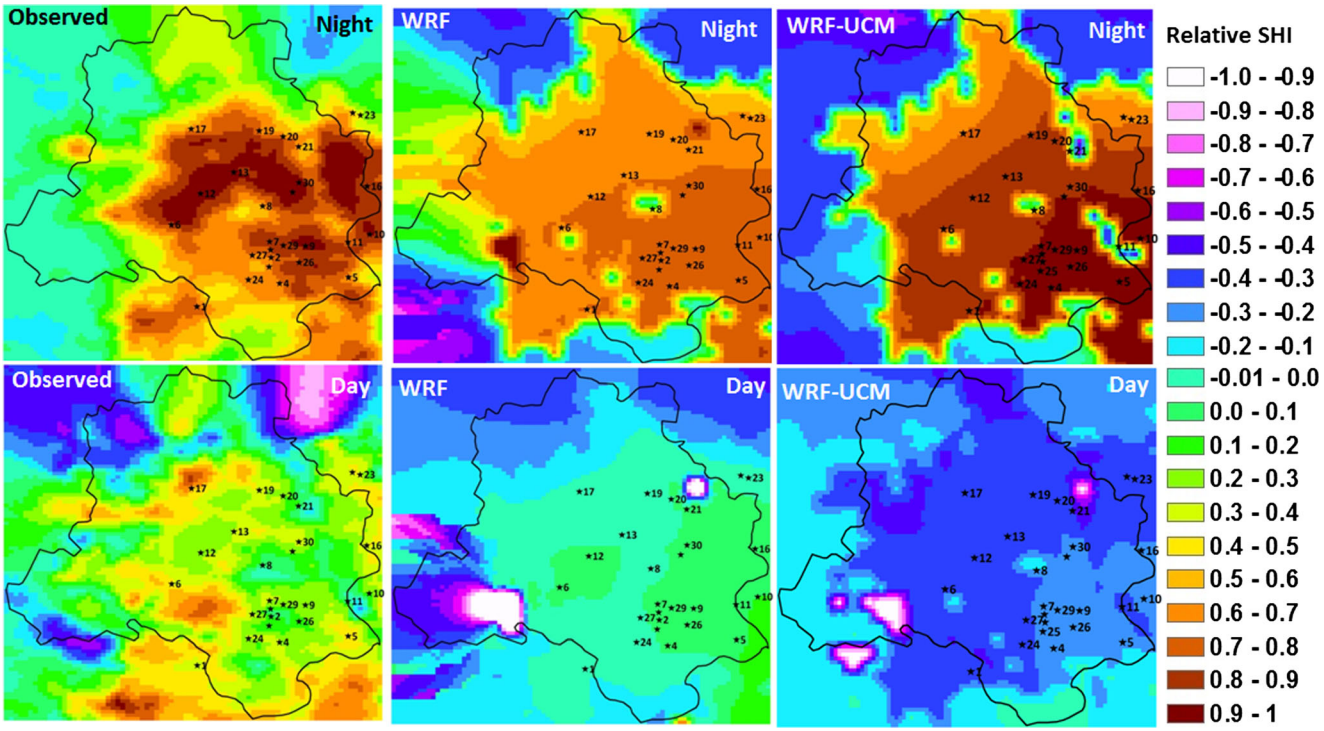

Fig. 11 Spatial distribution of UHI based on land surface temperature

themselves served as a different LULC type and were closely associated with high temperatures. Thus, SHI may be overestimated using satellite-based LSTs. Maximum SHI for observed distribution is 5.3 °C, while that from WRF and WRF-UCM distribution is 2.4 and −0.2 °C.

4 Conclusions

Urban heat island intensities have been assessed using WRF (version 3.5) model and WRF coupled with single-layer UCM for various land use/land cover prevalent in the subtropical urban Indian megacity of Delhi where it is found that WRF-UCM significantly improves the model performance both for meteorological parameters (T and RH) and the UHIs. Overall, RMSEs for near surface temperature improved from 1.63 to 1.13 °C for urban areas and from 2.89 to 2.75 °C for non-urban areas with inclusion of urban canopy model in WRF. Similarly, index of agreement and RMSEs for mean UHI improved from 0.77 to 0.88 and 1.91 to 1.60 °C, respectively, with WRF-UCM. Hit rates from the model-simulated mean heat island intensities using WRF model are 72 % for urban areas, 65 % for riverside, and 52 % for green areas. The corresponding values improved in WRF-UCM with a hit rate of 75 % for urban areas, followed by riverside (73 %) and green areas (71 %). In general, the model is able to capture the magnitude of UHI well though it performs better during night than during the daytime. Spatial distribution of UHI shows that major UHI hotspots and their intensities are well captured by WRF-UCM model. Both the WRF- and WRF-UCM-simulated UHIs show satisfactory performance against benchmarks for the statistical measures with classical methodology using rural site as a reference point. Using an alternate methodology for estimating the UHI considering a green area within the city having minimum temperature as a reference site worked satisfactorily only with WRF-UCM. Model performance comparisons with and without inclusion of urban canopy in the WRF model demonstrate that appropriate representation of urban canopies in the WRF model is important for predicting key features of mesoscale meteorology.

Acknowledgments The present study is a part of a research project "Implementation and Validation of Numerical Models for Heat Island Studies in Mega-city Delhi" conducted jointly by IIT Delhi, IIT Roorkee (Prof. B.R. Gurjar), and Meisei University, Tokyo (Prof. Y. Kikegawa). We thank The Ministry of Education, Culture, Sports, Science and Technology (MEXT), Japan for the partial financial support. We thank the participants of the field campaign from IIT Delhi, IIT Roorkee, and Meisei University. Some of the analyses in this study were based on data which were acquired as part of the NASA's Earth-Sun System Division and archived and distributed by the Goddard Earth Sciences (GES) Data and Information Services Center (DISC) Distributed Active Archive Center (DAAC). The authors would like to thank the anonymous reviewers for constructive suggestions that have helped in improving the quality of the paper.

References

Borge R, Alexandrov V, José del Vas J, Lumbreras J, Rodríguez E (2008) A comprehensive sensitivity analysis of the WRF model for air quality applications over the Iberian Peninsula. Atmos Environ 42: 8560–8574. doi:10.1016/j.atmosenv.2008.08.032

Chen F et al (2011a) The integrated WRF/urban modelling system: development, evaluation, and applications to urban environmental problems. Int J Climatol 31:273–288. doi:10.1002/joc.2158

Chen F, Miao S, Tewari M, Bao J-W, Kusaka H (2011b) A numerical study of interactions between surface forcing and sea breeze circulations and their effects on stagnation in the greater Houston area. Journal of Geophysical Research 116. doi:10.1029/2010jd015533

Chen F, Yang X, Zhu W (2014) WRF simulations of urban heat island under hot-weather synoptic conditions: the case study of Hangzhou City, China. Atmos Res 138:364–377. doi:10.1016/j.atmosres.2013.12.005

Ching JKS (2013) A perspective on urban canopy layer modeling for weather, climate and air quality applications. Urban Climate 3:13–39. doi:10.1016/j.uclim.2013.02.001

Cox R, Bauer BL, Smith T (1998) A mesoscale model intercomparison. Bull Am MeteorolSoc 79:265–283. doi:10.1175/1520-0477(1998)079<0265:AMMI>2.0.CO;2

Das PK (1968) The monsoons. National Book Trust, India

Ding H, Shi W (2013) Land-use/land-cover change and its influence on surface temperature: a case study in Beijing City. Int J Remote Sens 34:5503–5517. doi:10.1080/01431161.2013.792966

Dudhia J (1989) Numerical study of convection observed during the winter monsoon experiment using a mesoscale two-dimensional model. J Atmos Sci 46:3077–3107. doi:10.1175/1520-0469(1989)046<3077:NSOCOD>2.0.CO;2

Emery C, Tai E, Yardwood G (2001) Enhanced meteorological modeling and performance evaluation for two Texas ozone episodes. Environ International Corporation. http://www.tceq.state.tx.us/assets/public/implementation/air/am/contracts/reports/mm/EnhancedMetModelingAndPerformanceEvaluation.pdf. Accessed 15 October 2014

Emmanuel R, Krüger E (2012) Urban heat island and its impact on climate change resilience in a shrinking city: the case of Glasgow, UK. Build Environ 53:137–149. doi:10.1016/j.buildenv.2012.01.020

Fallmann J (2013) Modeling of the urban heat island (UHI) using WRF—assessment of adaptation and mitigation strategies for the city of Stuttgart. Paper presented at the EGU General Assembly Conference Abstracts, 2013

Flaounas E, Bastin S, Janicot S (2011) Regional climate modelling of the 2006 West African monsoon: sensitivity to convection and planetary boundary layer parameterisation using WRF. Clim Dyn 36:1083–1105. doi:10.1007/s00382-010-0785-3

Giannaros TM, Melas D, Daglis IA, Keramitsoglou I, Kourtidis K (2013) Numerical study of the urban heat island over Athens (Greece) with the WRF model. Atmos Environ 73:103–111. doi:10.1016/j.atmosenv.2013.02.055

Gilliam RC, Pleim JE (2010) Performance assessment of new land surface and planetary boundary layer physics in the WRF-ARW. J Appl Meteorol Climatol 49:760–774. doi:10.1175/2009JAMC2126.1

Giovanni (2014) Monsoon Asia Integrated Regional Study. National Aeronautics and Space Administration. http://gdata1.sci.gsfc.nasa.gov/daac-bin/G3/gui.cgi?instance_id=mairs_8day. Accessed 27 December 2014

Gupta M, Mohan M (2013) Assessment of contribution to PM10 concentrations from long range transport of pollutants using WRF/Chem over a subtropical urban airshed. Atmospheric Pollution Research 4:405–410. doi:10.5094/APR.2013.046

Hernández-Ceballos MA, Adame JA, Bolívar JP, De la Morena BA (2013) A mesoscale simulation of coastal circulation in the Guadalquivir valley (southwestern Iberian Peninsula) using the WRF-ARW model. Atmos Res 124:1–20. doi:10.1016/j.atmosres.2012.12.002

Hu X-M, Klein PM, Xue M, Lundquist JK, Zhang F, Qi Y (2013) Impact of low-level jets on the nocturnal urban heat island intensity in Oklahoma City. J Appl Meteorol Climatol 52:1779–1802. doi:10.1175/JAMC-D-12-0256.1

Huang X-Y et al (2009) Four-dimensional variational data assimilation for WRF: formulation and preliminary results. Mon Weather Rev 137:299–314. doi:10.1175/2008MWR2577.1

Imhoff ML, Zhang P, Wolfe RE, Bounoua L (2010) Remote sensing of the urban heat island effect across biomes in the continental USA. Remote Sens Environ 114:504–513. doi:10.1016/j.rse.2009.10.008

Jin MS (2012) Developing an index to measure urban heat island effect using satellite land skin temperature and land cover observations. J Clim 25:6193–6201. doi:10.1175/JCLI-D-11-00509.1

Kain JS (2004) The Kain–Fritsch convective parameterization: an update. J Appl Meteorol 43:170–181. doi:10.1175/1520-0450(2004)043<0170:TKCPAU>2.0.CO;2

Keramitsoglou I, Kiranoudis CT, Ceriola G, Weng Q, Rajasekar U (2011) Identification and analysis of urban surface temperature patterns in Greater Athens, Greece, using MODIS imagery. Remote Sens Environ 115:3080–3090. doi:10.1016/j.rse.2011.06.014

Khandelwal S, Goyal R, Kaul N (2010) Study of seasonal and spatial pattern of urban heat island of Jaipur City and its relationship with enhanced vegetation index. 13th Annual International Conference and Exhibition on Geospatial Information Technology and Applications. http://mapindia.org/2010/proceeding/pdf/186.pdf. Accessed 14 August 2014

Kim Y, Sartelet K, Raut J-C, Chazette P (2013) Evaluation of the weather research and forecast/urban model over greater Paris. Boundary-Layer Meteorol 149:105–132. doi:10.1007/s10546-013-9838-6

Kolokotroni M, Giannitsaris I, Watkins R (2006) The effect of the London urban heat island on building summer cooling demand and night ventilation strategies. Sol Energy 80:383–392. doi:10.1016/j.solener.2005.03.010

Kolokotroni M, Ren X, Davies M, Mavrogianni A (2012) London's urban heat island: impact on current and future energy consumption in office buildings. Energy Build 47:302–311. doi:10.1016/j.enbuild.2011.12.019

Kondo H, Genchi Y, Kikegawa Y, Ohashi Y, Yoshikado H, Komiyama H (2005) Development of a multi-layer urban canopy model for the analysis of energy consumption in a big city: structure of the urban canopy model and its basic performance. Boundary-Layer Meteorol 116:395–421. doi:10.1007/s10546-005-0905-5

Kusaka H, Kimura F (2004) Coupling a single-layer urban canopy model with a simple atmospheric model: impact on urban heat island simulation for an idealized case. Journal of the Meteorological Society of Japan Ser II 82:67–80. doi:10.2151/jmsj.82.67

Kusaka H et al (2012a) Numerical simulation of urban heat island effect by the WRF model with 4-km grid increment: an inter-comparison study between the urban canopy model and slab model. Journal of the Meteorological Society of Japan Ser II 90B:33–45. doi:10.2151/jmsj.2012-B03

Kusaka H, Hara M, Takane Y (2012b) Urban climate projection by the WRF model at 3-km horizontal grid increment: dynamical downscaling and predicting heat stress in the 2070's August for Tokyo, Osaka, and Nagoya metropolises. Journal of the Meteorological Society of Japan Ser II 90B:47–63. doi:10.2151/jmsj.2012-B04

Lee CB, Kim JC, Jang YJ (2012) A study of urban heat island in Chuncheon using WRF model and field measurements. Journal of Korean Society for Atmospheric Environment 28:119–130. doi:10.5572/KOSAE.2012.28.2.119

Leung LR, Qian Y (2009) Atmospheric rivers induced heavy precipitation and flooding in the western U.S. simulated by the WRF regional climate model. Geophys Res Lett 36:L03820. doi:10.1029/2008GL036445

Lin Y-L, Farley RD, Orville HD (1983) Bulk parameterization of the snow field in a cloud model. J Clim Appl Meteorol 22:1065–1092. doi:10.1175/1520-0450(1983)022<1065:BPOTSF>2.0.CO;2

Martin P, Baudouin Y, Gachon P (2014) An alternative method to characterize the surface urban heat island. Int J Biometeorol:1–13. doi:10.1007/s00484-014-0902-9

Masson V (2000) A physically-based scheme for the urban energy budget in atmospheric models. Bound Layer Meteorol 94:357–397. doi:10.1023/A:1002463829265

Meng WG, Zhang YX, Li JN, Lin WS, Dai GF, Li HR (2011) Application of WRF/UCM in the simulation of a heat wave event and urban heat island around Guangzhou. J Trop Meteorol 17:257–267

Mlawer EJ, Taubman SJ, Brown PD, Iacono MJ, Clough SA (1997) Radiative transfer for inhomogeneous atmospheres: RRTM, a validated correlated-k model for the longwave. J Geophys Res: Atmos 102:16663–16682. doi:10.1029/97JD00237

Mohan M, Bhati S (2011) Analysis of WRF model performance over subtropical region of Delhi, India. AdvMeteorol 2011 doi: 10.1155/2011/621235

Mohan M, Kikegawa Y, Gurjar BR, Bhati S, Kandya A, Ogawa K (2012) Urban heat island assessment for a tropical urban airshed in India. Atmos Clim Sci 2:12. doi:10.4236/acs.2012.22014

Mohan M, Kikegawa Y, Gurjar BR, Bhati S, Kolli N (2013) Assessment of urban heat island effect for different land use–land cover from micrometeorological measurements and remote sensing data for megacity Delhi. Theor Appl Climatol 112:647–658. doi:10.1007/s00704-012-0758-z

Myrup LO (1969) A numerical model of the urban heat island. J Appl Meteorol 8:908–918. doi:10.1175/1520-0450(1969)008<0908:ANMOTU>2.0.CO;2

NCAR (2013) User's guide for the advanced research WRF (ARW) modeling system version 3.5. http://www2.mmm.ucar.edu/wrf/users/docs/user_guide_V3/contents.html. Accessed 13 June 2013

Oke TR (1969) Towards a more rational understanding of the urban heat island. McGill Climatol Bull 5:1–21

Oke TR (1973) City size and the urban heat island. Atmos Environ (1967) 7:769–779. doi:10.1016/0004-6981(73)90140-6

Oke TR (1982) The energetic basis of the urban heat island. Q J Roy Meteorol Soc 108:1–24. doi:10.1002/qj.49710845502

Oleson KW, Bonan GB, Feddema J, Vertenstein M, Grimmond CSB (2008) An urban parameterization for a global climate model. Part I: formulation and evaluation for Two cities. J Appl Meteorol Climatol 47:1038–1060. doi:10.1175/2007JAMC1597.1

Pleim JE (2006) A simple, efficient solution of flux–profile relationships in the atmospheric surface layer. J Appl Meteorol Climatol 45:341–347. doi:10.1175/JAM2339.1

Pleim JE (2007) A combined local and nonlocal closure model for the atmospheric boundary layer. Part I: model description and testing. J Appl Meteorol Climatol 46:1383–1395. doi:10.1175/JAM2539.1

Porson A, Clark PA, Harman IN, Best MJ, Belcher SE (2010) Implementation of a new urban energy budget scheme in the MetUM. Part I: description and idealized simulations. Q J Roy Meteorol Soc 136:1514–1529. doi:10.1002/qj.668

Ramachandra TV, Kumar U (2010) Greater Bangalore: emerging urban heat island. GIS Development.http://www.ces.iisc.ernet.in/energy/paper/Bangalore_heatisland/index.htm. Accessed 27 Jul 2011

Ran L, Pleim J, Gilliam R (2010) Impact of high resolution land-use data in meteorology and air quality modeling systems. In: Steyn DG, Rao ST (eds) Air Pollution Modeling and its Application XX. Springer, Netherlands, pp 1–108. doi:10.1007/978-90-481-3812-8_1

Ren GY, Chu ZY, Chen ZH, Ren YY (2007) Implications of temporal change in urban heat island intensity observed at Beijing and Wuhan stations. Geophys Res Lett 34:L05711. doi:10.1029/2006GL027927

Santamouris M (2015) Analyzing the heat island magnitude and characteristics in one hundred Asian and Australian cities and regions. Sci Total Environ 512–513:582–598. doi:10.1016/j.scitotenv.2015.01.060

Sarrat C, Lemonsu A, Masson V, Guedalia D (2006) Impact of urban heat island on regional atmospheric pollution. Atmos Environ 40:1743–1758. doi:10.1016/j.atmosenv.2005.11.037

Shimadera H, Kondo A, Shrestha KL, Kaga A, Inoue Y (2011) Annual sulfur deposition through fog, wet and dry deposition in the Kinki Region of Japan. Atmos Environ 45:6299–6308. doi:10.1016/j.atmosenv.2011.08.055

Skamarock WC, Klemp JB, Dudhia J, Gill DO, Barker DM, Wang W, Powers JG. 2005. A description of the advanced research WRF version 2. NCAR Technical Note TN-468 + STR, 88 [Available from NCAR, P. O. Box 3000, Boulder, CO 80307

Steeneveld GJ, Koopmans S, Heusinkveld BG, van Hove LWA, Holtslag AAM (2011) Quantifying urban heat island effects and human comfort for cities of variable size and urban morphology in the Netherlands. J Geophys Res: Atmos 116:D20129. doi:10.1029/2011JD015988

Stewart ID (2011) A systematic review and scientific critique of methodology in modern urban heat island literature. Int J Climatol 31:200–217. doi:10.1002/joc.2141

Stewart ID, Oke TR (2009) A new classification system for urban climate sites. Bull Am Meteorol Soc 90:922–923

Stewart ID, Oke TR (2010) Thermal differentiation of local climate zones using temperature observations from urban and rural field sites. Ninth Symposium on Urban Environment, Keystone, CO, https://ams.confex.com/ams/pdfpapers/173127.pdf**. Accessed 14 October 2014**

Sundersingh SD (1990) Effect of heat islands over urban madras and measures for its mitigation. Energy Build 15:245–252. doi:10.1016/0378-7788(90)90136-7

Taha H (1997) Urban climates and heat islands: albedo, evapotranspiration, and anthropogenic heat. Energy and Buildings 25:99–103. doi:10.1016/S0378-7788(96)00999-1

Tan J et al (2010) The urban heat island and its impact on heat waves and human health in Shanghai. Int J Biometeorol 54:75–84. doi:10.1007/s00484-009-0256-x

Tewari M, Chen F, Wang W, Dudhia J, LeMone MA, Mitchell K, Ek M, Gayno G, Wegiel J, Cuenca RH (2004) Implementation and verification of the unified NOAH land surface model in the WRF model. 20th conference on weather analysis and forecasting/16th conference on numerical weather prediction, 11–15.

Tewari MF, Chen F, Kusaka H, Miao S (2007) Coupled WRF/Unified Noah/urban-canopy modeling system. NCAR WRF Documentation, NCAR, Boulder, pp 1–20, **Available online at** http://www.ral.ucar.edu/research/land/technology/urban/WRF-LSM-Urban.pdf

Tie X et al (2007) Characterizations of chemical oxidants in Mexico City: a regional chemical dynamical model (WRF-Chem) study. Atmos Environ 41:1989–2008. doi:10.1016/j.atmosenv.2006.10.053

Vázquez S, López Á, Souto JA, Casares JJ (2014) Validation of WRF model during O3 episodes in an Atlantic coastal region. In: Steyn DG, Builtjes PJH, Timmermans RMA (eds) Air pollution modeling and its application XXII. NATO Science for Peace and Security Series C: Environmental Security. Springer Netherlands, pp 599–603. doi:10.1007/978-94-007-5577-2_101

Wang X, Chen MF, Wu ZY, Zhang MG, Tewari M, Guenther A, Wiedinmyer C (2009) Impacts of weather conditions modified by urban expansion on surface ozone: comparison between the Pearl River Delta and Yangtze River Delta regions. Adv Atmos Sci 26:962–972. doi:10.1007/s00376-009-8001-2

Wang Z-H, Bou-Zeid E, Smith JA (2013) A coupled energy transport and hydrological model for urban canopies evaluated using a wireless sensor network. Q J Roy Meteorol Soc 139:1643–1657. doi:10.1002/qj.2032

Weng Q, Lu D, Schubring J (2004) Estimation of land surface temperature–vegetation abundance relationship for urban heat island studies. Remote Sens Environ 89:467–483. doi:10.1016/j.rse.2003.11.005

WMO (2008) Overview of tools and methods for meteorological and air pollution mesoscale model evaluation and user training. GAW Report No. 181. ftp://ftp.wmo.int/Documents/PublicWeb/arep/gaw/gaw181final_18dec08.pdf. Accessed 14 October 2014

Yuan F, Bauer ME (2007) Comparison of impervious surface area and normalized difference vegetation index as indicators of surface urban heat island effects in Landsat imagery. Remote Sens Environ 106:375–386. doi:10.1016/j.rse.2006.09.003

Zhang H, Sato N, Izumi T, Hanaki K, Aramaki T (2008) Modified RAMS-urban canopy model for heat island simulation in Chongqing, China. J Appl Meteorol Climatol 47:509–524. doi:10.1175/2007jamc1397.1

Zhang Y, Wen XY, Jang CJ (2010) Simulating chemistry–aerosol–cloud–radiation–climate feedbacks over the continental U.S. using the online-coupled Weather Research Forecasting Model with chemistry (WRF/Chem). Atmos Environ 44:3568–3582. doi:10.1016/j.atmosenv.2010.05.056